JOURNAL OF THEORETICAL BIOLOGY (USA)

Accepted 11 February 2016; Available online 21 February 2016

Impact Factor: 2.049; http://dx.doi.org/10.1016/j.jtbi.2016.02.011 0

ISSN: 0022-5193

BACTERIAL GLIDING FLUID DYNAMICS ON A LAYER OF NON-NEWTONIAN SLIME: PERTURBATION AND NUMERICAL STUDY

N. Ali[a,*], Z. Asghar[a], O. Anwar Bég[b] and M. Sajid[c]

[a] *Department of Mathematics and Statistics, International Islamic University, Islamabad 44000,* ***Pakistan.***

[b] *Fluid Mechanics Group, Mechanical and Aeronautical Engineering Department, Newton Building, The Crescent, Salford University, Manchester, M54WT,* ***England, UK.***

[c] *Theoretical Physics Division, PINSTECH, P.O. Nilore, Islamabad 44000,* ***Pakistan.***

Abstract:

Gliding bacteria are an assorted group of rod-shaped prokaryotes that adhere to and glide on certain layers of ooze slime attached to a substratum. Due to the absence of organelles of motility, such as flagella, the gliding motion is caused by the waves moving down the outer surface of these rod-shaped cells. In the present study we employ an undulating surface model to investigate the motility of bacteria on a layer of non-Newtonian slime. The rheological behavior of the slime is characterized by an appropriate constitutive equation, namely the Carreau model. Employing the balances of mass and momentum conservation, the hydrodynamic undulating surface model is transformed into a fourth-order nonlinear differential equation in terms of a stream function under the long wavelength assumption. A perturbation approach is adopted to obtain closed form expressions for stream function, pressure rise per wavelength, forces generated by the organism and power required for propulsion. A numerical technique based on an implicit finite difference scheme is also employed to investigate various features of the model for large values of the rheological parameters of the slime. Verification of the numerical solutions is achieved with a variational finite element method (FEM). The computations demonstrate that the speed of the glider decreases as the rheology of the slime changes from shear-thinning (pseudo-plastic) to shear-thickening (dilatant). Moreover, the viscoelastic nature of the slime tends to *increase* the swimming speed for the *shear-thinning* case. The fluid flow in the pumping (generated where the organism is not free to move but instead generates a net fluid flow beneath it) is also investigated in detail. The study is relevant to marine anti-bacterial fouling and medical hygiene biophysics.

Keywords: *Carreau non-Newtonian fluid, bacterial gliding, shear-thinning, shear-thickening, perturbation expansions, finite difference method (FDM), finite element method (FEM), propulsive force.*

*Corresponding author. Tel.: + 92 051 9019756; E-mail address: zeeshan.asghar@nu.edu.pk.

1. INTRODUCTION

Gliding is a mode of locomotion adopted by taxonomically heterogeneous rod-shaped prokaryotic bacteria on solid substrata. Gliding bacteria are generally Gram-negative and do not possesses

organelles of motility, such as flagella. Some common examples of gliding bacteria include vitresalla, oscillatoria, flexibector and cystobacter. The complex mechanisms by which these organisms achieve motility is still not fully understood, and such mechanisms may differ substantially among various species. Nearly all gliding bacteria as they move over a surface leave a trail of sticky liquid or slime [1]. Possible mechanisms of gliding which have been postulated include the presence of fimbriae-like appendages at the pole of gliding cell, generation of peristaltic waves, surface tension or pushing by secreted slime [2]. However, there is no conclusive evidence in support of any one particular mechanism of motility. Most of the gliding bacteria are less than $10\,\mu m$ long and $1\,\mu m$ in diameter. It is therefore not possible to make direct observations of their propulsion machinery. It is desired that any proposed mechanism of gliding motility must satisfy certain requirements in order to be acceptable. These are three-fold. Firstly the model must explain the *observed behavior* of the glider. Secondly the model must incorporate a *power requirement* for the motor. Thirdly the motor should be related to molecular structures within the organism [3-6]. It has been observed that gliding motility is often used by bacteria to their advantage. For instance, it helps many aerobic chemoheterotrophic bacteria to search for insoluble macromolecular substrates such as cellulose and chitin. Gliding is also well adapted to drier habitats and to movement within solid masses including soil, sediments and rotting wood. Furthermore, gliding motility enables bacteria to position themselves in optimal conditions of light intensity, oxygen, hydrogen sulphide, temperature and other environmental factors which significantly influence growth.

The available literature on morphology and gross behavior of certain glider for instance, vitreoscilla [4], oscillatoria [5-8] and flexibacter [9-11], supports an *undulating surface model* as a *feasible* mechanism of motility. It has been suggested that gliding may be caused by unidirectional surface waves travelling on the cell surface. These waves may be a result of lateral deformation of elements of a parallel array of fibrils ($50-80^0$ A wide) which have been found to be continuous over the surface of 300 mm wide trichome [12]. Jarosch [13] has proposed that the organism should be in contact with the solid substrate for gliding motility to occur, in which case the presence of this solid surface will serve as a structural base on which the motility mechanism of the trichome occurs.

Based on the above studies, O'Brien [14] carried out a mathematical analysis to investigate the fluid mechanism aspects of gliding motility caused by waves moving down the outer surface of

flexibacter, observing that for *any progressive waveform* there is an optimum distance from the wall at which the flexibacter may maximize its speed for a given power output. This investigation, nevertheless, did not incorporate any rheological features of the slime in the analysis. However, in a later study it was shown by Siddique *et al.* [15] that slime is a viscoelastic material that is composed of macromolecular polysaccharides, glycoproteins and proteins in an aqueous medium. It was further emphasized by Siddique *et al.* [15] that rheological features of slime may be quite diverse, and to this extent they explored, for the first time, the constitutive equation of third grade fluids (Reiner-Rivlin differential viscoelastic liquids) to mathematically simulate the rheological properties of the slime. Their analysis for non-Newtonian slime revealed that a lift force is generated due to the normal stresses. It was also shown that for a shear-thinning third-grade fluid, the power required for translation is reduced. Later attempts that incorporated shear-thinning/ shear thickening and viscoelastic nature of slime in undulating surface models for motility of gliding bacteria were made by Wang *et al.* [16] and Hayat *et al.* [17]. However, thusfar, no study is available in the mathematical biology or engineering biomechanics literature, in which an undulating surface model has been employed to study gliding motion of bacteria on a layer of non-Newtonian slime characterized by the Carreau fluid. The Carreau model uses three parameters (compared with two parameters in the power-law model). The additional parameter featured in the Carreau model is the material relaxation time (usually denoted by λ) which allows correlation with the molecular structure of the non-Newtonian liquid. It is therefore hoped that utilization of this model will more robustly represent the shear-thinning, shear thickening *and* viscoelastic properties of biological slime. Some recent studies dealing with flows of Carreau fluids can be found in refs. [18-20]. Moreover, it is strongly anticipated that the speed of the organism, forces generated by organism and power required for propulsion will be substantially influenced by the material relaxation time and the rheological power-law index. It is important to emphasize that the objective of the work is not merely a mathematical exercise. There is a great desire currently in, for example, the marine engineering (hydronautics) industry to develop intelligent materials for coating ocean-going vessels to counteract the compliant biofilms which are formed by bacteria in such environments [21]. Rheology has been shown to a be a critical factor in this regard [22] as it allows more effective development of synthetic materials for deployment in marine engineering systems e.g. offshore platforms, yacht hulls, pipelines etc. Similar interest is surfacing in microbiological engineering of waste treatment systems in civil engineering, biomimetic hydraulic

structures in hydropower systems and also lake regeneration initiatives. In this sense "smart" systems may be designed for reducing drag, mitigating corrosion, combatting slime adherence and other phenomena associated with bacterial and other aquatic/marine micro-organisms interacting with engineered devices [23]. The motivation of the present study is also, in part, due to some recent works carried out in the general area of microorganism swimming hydromechanics. In particular, Lauga *et al.* [24] have identified that near the solid surface, both force-free and toque-free swimming is responsible for the clockwise circular motion of micro-organism swimmers (cells) as well for their hydrodynamic vertical trapping. It has also been elucidated by Riley and Lauga [25] that the locomotion speed of micro-organisms is decreased, if all travelling waves move in same direction. However, an enhancement of the swimming speed has been observed if waves propagate in two opposite directions. The clockwise circular motion of the microorganism above the rigid surface and counterclockwise below the free surface, has been investigated in detail by Lopez and Lauga [26]. The results presented by Rusconi *et al*. [27] have revealed that the hydrodynamic environment may directly affect bacterial fitness and should be carefully considered in the study of microbial processes. A review of fluid physics governing the locomotion and feeding of individual planktonic microorganisms has been presented by Guasto *et al.* [28], largely orientated towards microbiological oceanic applications for civil engineering hydrosystem optimization. A comprehensive study of group micro-organism propulsion has been made by Koch and Subramanian [29] demonstrating that spontaneous motions may occur in systems of organisms induced by the coupling between the stresses generated by bacteria while swimming in fluids and furthermore the rotary motions of the bacteria arising as a result of the associated hydrodynamic disturbances. Further studies include the detailed simulations reported by Alouges *et al.* [30] dwelling on viscous-dominated optimization of micro-organism propulsion, Alouges *et al.* [31] concerning hydrodynamic efficiency of axisymmetric swimming of bacteria and Dal Maso *et al.* [32] on mathematical aspects of micro-organism swimming. All these investigations have emphasized the richness and complexity of bacterial hydrodynamics and re-charged this subject with a fresh motivation for new simulations with more sophisticated hydrodynamic models.

The structure of the present study is as follows: The geometry of the problem is illustrated in section 2. The equations governing the flow are described in section 3. The problem formulation and analytical expressions of pressure rise per wave length, forces generated by the organism and power required for propulsion valid for small Weissenberg number are presented in section 4. The

results based on numerical solution methodologies are expounded in section 5. Conclusions and future directions are elaborated in section 6. Details of the perturbation, finite difference and finite element solution techniques are documented in Appendix sections A, B and C respectively at the end of the article.

2. GEOMETRIC MODEL

Fig. 1 provides an illustrative diagram of the undulating sheet model utilized for the present mathematical simulation of bacterial gliding hydrodynamics. It is assumed that the bacterium is gliding over a flat surface and each point on the surface of the organism moves only in a direction transverse to the surface of the organism. The layer of exuded slime is pushed backward by the bacterium which generates a force that propels the bacterium in the direction opposite to the direction of the travelling wave. The glider will maintain a constant speed as a result of the balance between the work done by the waving sheet and the energy dissipated by the viscosity of the slime. Let V_g denote the propelling speed of the bacterium relative to the solid boundary and moving to the left, and let c denote the speed of the undulating wave relative to the organism and moving to the right. The apparent wave speed of the organism as viewed in a fixed co-ordinate frame is $(V_g - c)$. Let us choose a rectangular co-ordinate system (X, Y) with X -axis along the direction of propagation of waves and parallel to the substrate and Y -axis perpendicular to the substrate. The shape of the undulating surface, in this co-ordinate system, is expressed by:

$$h(X,t) = h_0 + a\,Sin\left[\left(\frac{2\pi}{\lambda}\right)\left(X - (c - V_g)\,\mathrm{t}\right)\right], \tag{1}$$

where λ is the wavelength, t is the time, h_0 denotes the mean distance of glider to the substratum and a is the amplitude.

3. HYDRODYNAMIC MODEL

The balances of mass and linear momentum for the flow of an incompressible fluid in vector form may be presented as:

$$\nabla . \boldsymbol{u} = 0, \tag{2}$$

$$\rho \frac{d\boldsymbol{u}}{dt} = \nabla . p + \nabla . \boldsymbol{S}, \tag{3}$$

where $\boldsymbol{u}$ is the fluid velocity, ρ is the density, $\boldsymbol{S}$ is the extra stress tensor and d/dt is the material time derivative. Let the rheological properties of the slime be represented by the Carreau model. The appropriate extra stress tensor $\boldsymbol{S}$ becomes [18-20]:

$$\boldsymbol{S} = \left(\mu_\infty + \left(\mu_0 - \mu_\infty \right) \left[1 + \Gamma^2 \Pi^2 \right]^{\frac{n-1}{2}} \right) \boldsymbol{A}_1. \tag{4}$$

In Eqn. (4) μ_∞ is the infinite shear-rate viscosity, μ_0 is the zero shear rate viscosity, Γ is the time constant, n is the rheological power law index, $\boldsymbol{A}_1$ is the first Rivilin-Ericksen tensor and Π is given by:

$$\Pi = \sqrt{\frac{1}{2} tr\left(\boldsymbol{A}_1^2 \right)}. \tag{5}$$

For the subsequent analysis, we shall assume that $\mu_\infty = 0$.

4. PROBLEM FORMULATION

Consider the unsteady, two-dimensional, laminar flow of an incompressible Carreau fluid in the form of a thin layer of slime. The velocity field for two-dimensional flow is given by:

$$\boldsymbol{V} = \left[U\left(X, Y, t \right), V\left(X, Y, t \right), 0 \right], \tag{6}$$

where U and V are respective velocity components in X and Y directions. In view of Eqn. (6), the continuity Eqn. (2), the momentum Eqn. (3) and component of extra stress $\boldsymbol{S}$ take the following form:

$$\frac{\partial U}{\partial X} + \frac{\partial V}{\partial Y} = 0, \tag{7}$$

$$\rho \left(\frac{\partial}{\partial t} + U \frac{\partial}{\partial X} + V \frac{\partial}{\partial Y} \right) V = -\frac{\partial p}{\partial X} + \frac{\partial S_{XY}}{\partial X} + \frac{\partial S_{YY}}{\partial Y}, \tag{8}$$

$$\rho\left(\frac{\partial}{\partial t}+U\frac{\partial}{\partial X}+V\frac{\partial}{\partial Y}\right)V=-\frac{\partial p}{\partial Y}+\frac{\partial S_{XY}}{\partial X}+\frac{\partial S_{YY}}{\partial Y}, \tag{9}$$

$$S_{XX}=2\mu_0\left[1+\Gamma^2\Pi^2\right]^{\frac{n-1}{2}}\left(\frac{\partial U}{\partial X}\right), \tag{10}$$

$$S_{XY}=\mu_0\left[1+\Gamma^2\Pi^2\right]^{\frac{n-1}{2}}\left(\frac{\partial U}{\partial Y}+\frac{\partial V}{\partial X}\right), \tag{11}$$

$$S_{YY}=2\mu_0\left[1+\Gamma^2\Pi^2\right]^{\frac{n-1}{2}}\left(\frac{\partial V}{\partial Y}\right), \tag{12}$$

where

$$\Pi^2=2\left[\left(\frac{\partial U}{\partial X}\right)^2+\left(\frac{\partial V}{\partial Y}\right)^2\right]+\left(\frac{\partial U}{\partial Y}+\frac{\partial V}{\partial X}\right)^2. \tag{13}$$

In the fixed frame, the adherence boundary conditions may be simulated as follows:

$$\begin{aligned} &U=-V_g \ \text{ at } \ Y=h, \\ &U=0 \ \text{ at } \ Y=0. \end{aligned} \tag{14}$$

Let us define the following transformations to switch from the *fixed frame* (X,Y) to the *wave frame* (x,y). This co-ordinate transformation is advantageous since flow phenomena in the wave frame become *steady* and the boundary shape appears to be *stationary*:

$$\begin{aligned} &x=X-(c-V_g)t, \quad y=Y, \\ &u=U-(c-V_g), \quad v=V, \end{aligned} \tag{15}$$

where u, v are the respective velocity components in the x and y directions. Implementing the above transformations, we simultaneously introduce the following dimensionless variables and numbers:

$$\begin{aligned} &x^*=\frac{2\pi}{\lambda}x, \quad y^*=\frac{y}{h_0}, \quad u^*=\frac{u}{c}, \quad v^*=\frac{v}{\delta c}, \quad h^*=\frac{h(x)}{h_0}, \quad p^*=\frac{2\pi h_0^2}{\lambda\mu_0 c}p, S_{xx}^*=\frac{h_0}{\mu_0 c}S_{xx}, \\ &S_{xy}^*=\frac{h_0}{\mu_0 c}S_{xy}, S_{yy}^*=\frac{2\pi h_0^2}{\lambda\mu_0 c}S_{yy}, \ \Pi^*=\frac{h_0}{c}\Pi, \ \ \delta=\frac{2\pi h_0}{\lambda}, \ \ R_e=\frac{\rho c h_0}{\mu_0}, \ \ We=\frac{\Gamma c}{h_0}, \end{aligned} \tag{16}$$

Furthermore we define a dimensionless stream function as follows:

$$u = \frac{\partial \psi}{\partial y}, \quad v = -\frac{\partial \psi}{\partial x}, \tag{17}$$

Omitting the superscript * for convenience, we find that the continuity Eqn. (7) is identically satisfied and Eqns. (8)-(13) reduce to:

$$\delta R_e \left[\left(\frac{\partial \psi}{\partial y}\frac{\partial}{\partial x} - \frac{\partial \psi}{\partial x}\frac{\partial}{\partial y} \right)\left(\frac{\partial \psi}{\partial y} \right) \right] + \frac{\partial p}{\partial x} = \delta \frac{\partial}{\partial x} S_{xx} + \frac{\partial}{\partial y} S_{xy}, \tag{18}$$

$$-\delta^3 R_e \left[\left(\frac{\partial \psi}{\partial y}\frac{\partial}{\partial x} - \frac{\partial \psi}{\partial x}\frac{\partial}{\partial y} \right)\left(\frac{\partial \psi}{\partial x} \right) \right] + \frac{\partial p}{\partial y} = \delta^2 \frac{\partial}{\partial x} S_{xy} + \frac{\partial}{\partial y} S_{yy}, \tag{19}$$

$$S_{xx} = 2\delta \left[1 + We^2 \Pi^2 \right]^{\frac{n-1}{2}} \left(\frac{\partial^2 \psi}{\partial x \partial y} \right), \tag{20}$$

$$S_{xy} = \left[1 + We^2 \Pi^2 \right]^{\frac{n-1}{2}} \left(\frac{\partial^2 \psi}{\partial y^2} - \delta^3 \frac{\partial^2 \psi}{\partial x^2} \right), \tag{21}$$

$$S_{yy} = -2\delta^3 \left[1 + We^2 \Pi^2 \right]^{\frac{n-1}{2}} \left(\frac{\partial^2 \psi}{\partial x \partial y} \right), \tag{22}$$

where

$$\Pi = \left[\left(2\delta \frac{\partial^2 \psi}{\partial x \partial y} \right)^2 + \left(\frac{\partial^2 \psi}{\partial y^2} - \delta^2 \frac{\partial^2 \psi}{\partial x^2} \right)^2 \right]^{\frac{1}{2}}. \tag{23}$$

In the above equations, δ is the dimensionless wave number, R_e is the Reynolds number and We is the Weissenberg number (characterizing rheology of the slime). Eliminating pressure between Eqns. (18) and (19), we obtain:

$$R_e \delta \left(\frac{\partial \psi}{\partial y}\frac{\partial}{\partial x} - \frac{\partial \psi}{\partial x}\frac{\partial}{\partial y} \right)\left(\frac{\partial^2 \psi}{\partial y^2} + \delta^2 \frac{\partial^2 \psi}{\partial x^2} \right) = \left(\frac{\partial^2 S_{xy}}{\partial y^2} - \delta^2 \frac{\partial^2 S_{xy}}{\partial x^2} \right) + \frac{\partial^2}{\partial x \partial y}\left(\delta S_{xx} - S_{yy} \right). \tag{24}$$

The subsequent analysis is based on the assumption that $\delta<<1$. This assumption is known as the *long wave length assumption* in the literature and is popular in lubrication theory and other areas including bacterial transport phenomena modelling [14-17] and peristaltic propulsion [33, 34]. In view of this assumption, Eqn. (24) reduces to:

$$\frac{\partial^2}{\partial y^2}\left[\left(1+We^2\left(\frac{\partial^2\psi}{\partial y^2}\right)^2\right)^{\frac{n-1}{2}}\left(\frac{\partial^2\psi}{\partial y^2}\right)\right]=0. \tag{25}$$

Similarly, we can write Eqn. (18) as follows:

$$\frac{\partial p}{\partial x}=\frac{\partial}{\partial y}\left[\left(1+We^2\left(\frac{\partial^2\psi}{\partial y^2}\right)^2\right)^{\frac{n-1}{2}}\left(\frac{\partial^2\psi}{\partial y^2}\right)\right]. \tag{26}$$

Eqn. (25) is subject to following boundary conditions [15]:

$$\begin{aligned}&\psi=0,\ \ \frac{\partial\psi}{\partial y}=V_b \quad at\ \ y=0,\\ &\psi=F,\ \ \frac{\partial\psi}{\partial y}=-1 \quad at\ \ y=h=1+\phi\sin x,\end{aligned} \tag{27}$$

where $\phi\left(=\frac{a}{h_0}\right)$ is the occlusion parameter, $V_b=\frac{V_g}{c}-1$ and F is the dimensionless mean flow rate in the *wave frame*. The dimensionless mean flow rate Θ, in the *fixed frame* is related to F according to the simple relation:

$$\Theta=F-V_b. \tag{28}$$

With the objective of deriving analytical expressions of pressure rise per wavelength, forces generated by the gliding bacteria and the power required for propulsion, a perturbation approach valid for small values of We is employed. For large values of We, recourse to an implicit finite difference method (FDM) is required. The results obtained via FDM are further verified by variational finite element method (FEM). Details of analytical as well as the alternative numerical (FDM) procedure to achieve computational solutions of the problem and furthermore validation of the FDM graphical computations with a robust variational finite element method (FEM), for

fixed values of the speed of the organism, are all documented in sections A, B and C of the Appendix.

For small values of We, the expression of $\Delta P^{(1)}{}_{\lambda}$ can be written in the following form:

$$\Delta P^{(1)}{}_{\lambda} = -6\left(\mathrm{I}_2 + 2F^{(1)}I_3 - I_2V_b\right) + \frac{18}{5}(n-1)We^2\Big[-7I_4 - 2F^{(1)}\left(16I_5 + 9F\left(3I_6 + 2FI_7\right)\right) + V_b\left(11I_4 + 44F^{(1)}I_5 + 54\left(F^{(1)}\right)^2 I_6 + V_b\left(-11I_4 - 32F^{(1)}I_5 + 7I_4V_b\right)\right)\Big]. \tag{29}$$

The organism will maintain a steady speed at a fixed distance from the substrate only when net forces in the longitudinal and transverse direction are zero. Additionally, we may assume pressure difference per wavelength to be zero [14, 15]. The resulting expression of *horizontal* and *vertical* forces *per unit width per wavelength* on the surface of the organism and power required for gliding of the organism at a steady speed V_b, valid to the first order in We, are given by:

$$F_x^{(1)} = 2\left(I_1 + 3F^{(1)}I_2 - 2I_1V_b\right) - \frac{2}{5}(n-1)We^2\Big[-19I_3 - 9F^{(1)}\left(11I_4 + 2F^{(1)}\left(11I_5 + 9F^{(1)}I_6\right)\right) + V_b\left(6\left(7I_3 + 33F^{(1)}I_4 + 48\left(F^{(1)}\right)^2 I_5\right) + V_b\left(-57I_3 - 189F^{(1)}I_4 + 44I_3V_b\right)\right)\Big], \tag{30}$$

$$F_y^{(1)} = 0, \tag{31}$$

$$P^{(1)} = -F_x^{(1)}. \tag{32}$$

Now in order to obtain the steady speed maintained by the glider, we equate each of the quantities $F_x^{(1)}$, $F_y^{(1)}$ and $\Delta P^{(1)}{}_{\lambda}$ to zero and seek a *unique set of rules* such that $0 \le \varphi < 1$; $F^{(1)} < 0$ and $V_b < 0$. It is noted that, similar to the Newtonian case, the *lift force* generated by the Carreau slime is *zero*. Therefore, similar to the Newtonian case, there is only one degree of freedom. Due to the non-linear expressions for $F_x^{(1)}$ and $\Delta P^{(1)}{}_{\lambda}$ it is possible to find closed form expressions of V_b and $F^{(1)}$. However, for given values of ϕ, We and n, plausible numerical values of V_b and $F^{(1)}$ must be found using symbolic softwares such as Mathematica or Matlab. The results obtained with this approach are plotted in Figs. 2(a)-(c). Fig. 2(a) shows the variation of speed of the organism with respect to the power-law index for fixed values of ϕ and We. This figure demonstrates that the speed of the organism *decreases* as the rheology of the slime changes from *shear-thinning* to

shear-thickening. Fig. 2(b) illustrates that speed increases with an increase in the occlusion parameter. The variation of the speed of the organism with respect to Weissenberg (We) is shown for both shear-thinning and shear-thickening fluids in Fig. 2(c). As expected the organism maintains a constant speed for $n=1$ (Newtonian case). For shear-thinning fluid an increase in We decreases the speed. On the contrary, the speed of the organism increases with increasing We for shear-thickening fluid.

5. FDM NUMERICAL RESULTS AND DISCUSSION

The finite difference method (FDM), a robust computational technique, has been implemented to solve the boundary value problem defined by eqn. (25) under boundary conditions (27) and results generated are displayed for several values of the hydrodynamic control parameters. The computations are also carried out for $V_b \le -1$. As far as the problem of gliding motility of the organism is concerned, $V_b > -1$. The assumption for the case $V_b = -1$ correspond to the case of pumping transportation of fluid by the wavy motion of the upper wall. In other words the case $V_b = -1$ corresponds to the flow problem of a *slime layer between the organism and the substrate*. However, in order not to resist our investigations for $V_b = -1$, numerical results for $V_b < -1$ are also displayed. The result presented here are also appropriate to the channel flow of Carreau fluid between two walls or between one plate and a wavy surface with corresponding boundary conditions.

Fig. 3(a) illustrate the velocity profiles at a cross-section $x=\pi$ for different values of n corresponding to *three different values of prescribed flow rate* F for $V_b = 0$ and $We = 7$. It is noted that for $F = -0.5$, the velocity varies linearly with respect to y. In this case, the curves for different values of n coincide i.e. for this specific choice of flow rate the velocity at this cross-section is *independent* of the power-law index, n. For $F = 1$, the velocity at this cross-section varies in a nonlinear function with respect to y. In this case, the longitudinal velocity exhibits boundary layer character for $n = 0.1$ (strong shear-thinning i.e. pseudoplastic fluid). The largest gradients in velocity occur at the boundary region for this case and the middle-most region out of the thin boundary layers moves as though it were a *plug flow*. The boundary layer thicknesses formed at either wall ($y = 0$ or $y = h$) are found to be *inversely* proportional to $|V_b|$. On the contrary, the

shearing effects near the boundaries extend to the whole domain with increasing power-law index (i.e. for $n = 0.76, 1, 1.24$). In these cases, no sharp boundary layer exists at either wall. This fact is delineated in **Fig. 3(b)**. It is further noted from Fig. 3 that the magnitude of velocity in the central part of the gap between the wavy wall and the substrate *increases* with *increasing* power-law index. A converse trend is noted in the vicinity of the walls.

The effects of Weissenberg number on longitudinal velocity at a cross-section $x = \pi$ for different values of *We* corresponding to three values of flow rate F for $V_b = 0$ and $n = 0.8$ are shown in **Fig. 4(a)**. It is observed that the longitudinal velocity in the central part of the domain $y \in [0, h]$ decreases by increasing *We*. The profiles of longitudinal velocity for shear-thickening fluid with similar parameter values, as used in **Fig. 4(a)**, are shown in **Fig. 4(b)**. It is found that longitudinal velocity exhibits the converse trend with increasing *We* for a shear-thickening fluid i.e. its magnitude in the vicinity of the central part increases with increasing *We*. A comparison of velocity profiles for *Newtonian* and *Carreau* fluids can also be made via examination of Figs. 3 and 4. Generally, it is observed that the longitudinal velocity in the case of Carreau fluid exhibits a behavior which is similar to the velocity of Newtonian fluid in a qualitative sense *provided that the Weissenberg number is sufficiently small*. In the quantitative sense, the Carreau model predicts higher values of longitudinal velocity in comparison with the Newtonian model depending on the nature of fluid. For shear-thinning Carreau fluid, the magnitude of the longitudinal velocity is higher than the magnitude of longitudinal velocity for a Newtonian fluid. The longitudinal velocity based on the Carreau model for the shear-thinning case, with greater Weissenberg number, shows significant quantitative deviation from the corresponding velocity for the Newtonian model. In such a situation, contrary to the Newtonian case, the velocity for the Carreau model is characterized by formation of thin boundary layers near the walls

The relationship between pressure rise per wavelength and flow rate for the case when the organism is restrained and its oscillatory motion entrains a net fluid flow along the *x* direction, is shown in **Figs. 5 and 6** for different values of power-law index and Weissenberg number, respectively

Fig. 5 reveals that pressure rise per wavelength in the pumping region ($\Delta p > 0, \Theta > 0$) is elevated with increasing power-law index. In other words pressure rise increases in going from shear-thinning to shear-thickening fluids. The *free pumping* flux i.e Θ for $\Delta p = 0$ is also found to increase when fluid behavior changes from shear-thinning to shear-thickening. It is also interesting

to note that in the *co-pumping* region ($\Delta p < 0, \Theta > 0$), the magnitude of pressure rise per wavelength also increases as we progress from shear-thinning to shear-thickening fluids. Moreover, for an appropriately chosen $\Delta p < 0$, the pumping flux *increases* from the shear-thickening scenario to the shear-thinning fluids.

The pressure rise per wavelength plotted against flow rate (Θ) for different values of We is shown in **Fig. 6(a)** for a shear-thinning fluid. Here it is found that Δp in the pumping region decreases with increasing We. The curve for a Newtonian fluid lies below all other curves corresponding to different values of We. In this way, the organism has to work against greater pressure rise to maintain the same flux for a Newtonian slime in comparison to a slime with shear-thinning properties. On the contrary, **Fig. 6(b)** implies that in the shear-thickening case the curve for Newtonian fluid lies below all other curves corresponding to different values of We. This indicates that much greater effort is rendered by the organism to maintain the same flux with the change in rheological properties of slime from Newtonian to shear-thickening.

The patterns of streamlines for different values of power-law index and Weissenberg number when $V_b = -1$ and $F = 0.5$ are shown in **Fig. 8**. Generally, it is observed that streamlines near either boundary *assume the shape of that boundary*. However, in the central region, circulating eddies emerge depending on the value of prescribed flow rate. **Fig. 8(a)** illustrates the streamlines pattern for three different values of We corresponding to slime exhibit shear-thinning rheological behavior. A small eddy is found in the central region of flow field for $We = 0$ (Newtonian fluid). The size of this eddy is found to diminish by increasing We and eventually the eddy disappears for large values of We. **Fig. 8(b)** depicts that for the shear-thickening fluid case ($We = 0.5, n = 1.2$) the size of the eddy which was originally present for a Newtonian fluid, increases and *another eddy* appears near the undulating surface. It is further observed that both the eddies grow larger in size for higher values of We. The patterns of streamlines of different values of power-law index are shown in **Fig. 9**. This figure confirms the appearance of a single eddy in the central region for $n = 0.2$. The size of eddy increases with increasing the value of n from 0.2 to 1. For $n = 1.5$, the eddy in the central region grow further in size and another eddy appears near the undulating surface. It is anticipated that size of both eddies grows further with increasing *n.* Overall, the influence of *slime rheology* is significant on the fluid dynamic characteristics.

6. CONCLUDING REMARKS

An undulating surface model for gliding motion of bacteria has been developed for the case when gap width between the organism and substrate is small as compared to the organism, and the substrate is small as compared to the wavelength of the undulating wave on the organism surface. A perturbative analysis is carried out to estimate the speed of organism as a function of rheological parameters of the slime and amplitude of the undulating wave. Numerical computations based on the finite difference method are also carried out to analyze the pumping problem, where the sheet is not allowed to move and its oscillatory motion entrains a net fluid flow along the *x*-direction. Validation of the finite difference method (FDM) solutions is achieved with a variational finite element method (FEM). Excellent correlation is attained. The important deductions from the present mathematical and computational study may be summarized as follows.

- For a fixed Weissenberg number, the gliding speed of the bacteria *decreases* with a change in rheological properties of the slime from shear-thinning to shear-thickening.
- For shear-thinning of slime, the speed of the organism *increases* with increasing Weissenberg number. However, a converse trend is noted for an organism gliding on shear-thickening slime.
- The speed of the organism is an *increasing* function of the amplitude of the undulating wave.
- For *small values of the amplitude* of the undulating wave, the speed of the organism is *independent* of the rheological properties of the slime.
- For slime with *strong shear-thinning properties*, the flow exhibits boundary layer characteristics. In this case, the largest gradients in velocity are confined to thin layers near the substrate and the organism surface while the flow in the central zone is uniform.
- For $V_b = 0$ (the case in which organism is held fixed), it is found that greater effort is expended by the organism to maintain the constant flux with the change in the rheological properties of the slime from Newtonian to shear-thickening.
- For $V_b = 0$ the circulation of fluid in the central region between the substrate an undulating surface increases from the shear-thinning to shear-thickening case.

- For the shear-thinning case with $V_b = 0$, an increase in Weissenberg number decreases the circulation of the fluid in the central region. A converse trend is observed for shear-thickening slime.

The present study may be further generalized to consider more complex rheological models e.g. micro-continuum models [35] which consider micro-structural features of the slime (e.g. rotary motions of micro-elements) and also *inclined* surface glider dynamics. These are presently being addressed. The present perturbation, FDM and FEM approaches all appear to hold excellent promise for these more complex simulations.

REFERENCES

[1] R.P. Burchard, Gliding motility and taxes, in: *E. Rosenberg (Ed.), Myxobacteria: Development and Cell Interactions*, Springer, Berlin, (1984) 139-161.

[2] J.L. Pate, Gliding motility in prokaryotic cells, *Can. J. Microbiol*. **34** (1988) 459-465.

[3] A.C. Burchard, R.P. Burchard, J.A. Kloetzel, Intracellular, periodic structures in the gliding bacterium Myxococcus Xanthus, *J. Bacteriol*. **132** (1977) 666-672.

[4] J.W.F. Costerton, CF Murray, Robinow, Observations on the motility and the structure of Vitreoscilla, *Can. J. Microbiol*. **7** (1961) 329-339.

[5] L.N. Halfen, R.W. Castenholz, Gliding in the blue-green alga: a possible mechanism, *Nature*, **225** (1970) 1163-1165.

[6] L.N. Halfen, Gliding motility of Oscillatoria, ultrastructural and chemical characterization of the fibrillar layer, *J. Phycol*. **9** (1970) 248-253.

[7] E.J. Ambrose, The movement of fibrocytes, *Exp. Cell Res.Suppl*. **9** (1961) 54-73.

[8] L.N. Halfen, R.W. Castenholz, Gliding in the blue-green alga, *J. Phycol*. **7** (1971) 133-144.

[9] B.A. Humphrey, M.R. Dickson, K.C. Marshall, Physicochemical and in situ observations on the adhesion of gliding bacteria to surfaces, *Arch. Microbiol*. **120** (1979) 231-238.

[10] M.R. Dickson, S. Kouprach, B.A. Humphrey, K.C. Marshall, Does gliding motility depend on undulating membranes? *Micron* **11** (1980) 381-382.

[11] T. Duxbury, B.A. Humphrey, K.C. Marshall, Continuous observations of bacterial gliding motility in a dialysis micro-chamber: the effects of inhibitors, *Arch. Microbiol*. **124** (1980) 169-175.

[12] L.N. Halfen, R.W. Castenholz. Gliding in a blue-green: a possible mechanism. *Nature* **225** (1970), 1163–1165.

[13] R. Jarosch. *Gliding. In physiology and biochemistry of Algae, Lewin RA. (ed)* Academic Press: New York. (1962) 573-581.

[14] R.W. O'Brien. The gliding motion of a bacterium, Flexibactor strain BH 3, *J. Australian Mathematical Society (Series B)* **23 (**1981) 2–16.

[15] A.M. Siddiqui, R.P. Burchard and W.H. Schwarz. An undulating surface model for the motility of bacteria gliding on a layer of non-Newtonian slime, *Int. J. Non-Linear Mechanics.* **36** (2001) 743–761.

[16] Y. Wang, T. Hayat and A.M. Siddiqui. Gliding motion of bacteria on a power–law slime. *Mathematical Methods of Applied Science,* **28** (2005) 329–347.

[17] T. Hayat, Y. Wang, A.M. Siddiqui and S.Asghar. A mathematical model for the study of gliding motion of bacteria on a layer of non–Newtonian slime. *Mathematical Methods in the Applied Sciences.* **27** (2004) 1447–1468.

[18] N. Ali, K. Javid, M. Sajid and O. Anwar Beg. Numerical simulation of peristaltic flow of a bio rheological fluid with shear-dependent viscosity in a curved channel. *Computer Methods in Biomechanics and Biomedical Engineering*, DOI: 10.1080/10255842.2015. 1055257

[19] A. Zaman, N. Ali, M. Sajid and T. Hayat. Effects of unsteadiness and non-Newtonian rheology on blood flow through a tapered time-variant stenotic artery. *AIP advances*, DOI: 10.1063/1.4916043.

[20] N. Ali, A. Zaman, M. Sajid, J.J. Nieto and A. Torres. Unsteady non-Newtonian blood flow through a tapered overlapping stenosed catheterized vessel. *Mathematical Biosciences* **269** (2015) 94-103.

[21] P. Shivapooja, Wang, Q., Orihuela, B., Rittschof, D., López, G. P. and Zhao, X., Bioinspired surfaces with dynamic topography for active control of biofouling. *Adv. Mater*., **25** (2013) 1430-1434.

[22] P. Majumdar, A. Ekin and D.C. Webster, Thermoset siloxane-urethane fouling release coatings, *Smart Coatings, Eds (T. Provder and J. Baghdachi), American Chemical Society*, 61-75 (2007).

[23] D.M. Yebra, S.N. Rasmussen, C. Weinell and L.T. Pedersen, Marine fouling and corrosion protection for offshore ocean energy setups, *3rd Int. Conf. Ocean Energy, Bilbao, Spain, October 6* (2010).

[24] E. Lauga, W.R. DiLuzio, G.M. Whitesides and H.A. Stone, Swimming in circles: motion of bacteria near solid boundaries, *Biophysical J.*, **90** (2006) 400–412.

[25] E.E. Riley and E.Lauga, Small-amplitude swimmers can self-propel faster in viscoelastic fluids, *J. Theoretical Biology*, **382** 345–355 (2015).

[26] D. Lopez and E. Lauga, Dynamics of swimming bacteria at complex interfaces, *Physics of Fluids*, **26** 071902 (2014).

[27] R. Rusconi, J.S. Guasto and R.Stocker, Bacterial transport is suppressed by fluid shear. *Nature Physics*, **10** 212-217 (2014).

[28] J.S. Guasto, R. Rusconi and R. Stocker, Fluid mechanics of planktonic micro-organisms. *Ann. Rev. Fluid Mech*. **44** 373–400 (2012).

[29] D. L. Koch and G. Subramanian, Collective hydrodynamics of swimming microorganisms: living fluids, *Ann. Rev. Fluid Mechanics*, 43 (2011) 637-659.

[30] F. Alouges, A. DeSimone, A. Lefebvre, Optimal strokes of low Reynolds number swimmers: an example, *J. Nonlinear Science*, 18 (2008) 277-302.

[31] F. Alouges, A. DeSimone, A. Lefebvre, Optimal strokes of axisymmetric microswimmers, *European Physical Journal E,* 28 (2009) 279–284.

[32] G. Dal Maso, A. DeSimone, M. Morandotti: An existence and uniqueness result for the self-propelled motion of micro-swimmers, *SIAM J. Math. Analysis*, 43 (2011) 1345-1368.

[33] H.S. Lew, Y.C. Fung and C.B. Lowenstein, Peristaltic carrying and mixing of chyme in small intestine, *J. Biomechanics*. **4** (1971) 297-315.

[34] N. Ali, A. Abbasi and I. Ahmad. Channel flow of Ellis fluid due to peristalsis, *AIP Advances*. **5** (2015) 097214.

[35] N. Ali, A. Zaman and O. Anwar Bég, Numerical simulation of unsteady micropolar hemodynamics in a tapered catheterized artery with a combination of stenosis and

aneurysm, *Medical and Biological Engineering and Computing* (2015). DOI: 10.1007/s11517-015-1415-3.

[36] P. Rana, R. Bhargava and O. Anwar Bég, Finite element modeling of conjugate mixed convection flow of Al_2O_3-water nanofluid from an inclined slender hollow cylinder, *Physica Scripta*, **88** (2013) (15pp).

[37] R. Bhargava, S. Sharma, O. Anwar Bég and Zueco, J, Finite element study of nonlinear two-dimensional deoxygenated biomagnetic micropolar flow, *Communications in Nonlinear Science and Numerical Simulation*, 15 (2010) 1210-1233.

[38] D. Gupta, L. Kumar, O. Anwar Bég and B. Singh, Finite element simulation of mixed convection flow of micropolar fluid over a shrinking sheet with thermal radiation, *Proc IMechE- Part E: J. Process Mechanical Engineering*, 228 (2014) 61-72.

[39] O. Anwar Bég, Tasveer A. Bég, R. Bhargava, S. Rawat and D. Tripathi, Finite element study of pulsatile magneto-hemodynamic non-Newtonian flow and drug diffusion in a porous medium channel, *J. Mechanics in Medicine and Biology*, 12 (2012) 1250081.1 – 1250081.26.

[40] P. Rana and O. Anwar Bég, Mixed convection flow along an inclined permeable plate: effect of magnetic field, nanolayer conductivity and nanoparticle diameter, *Applied Nanoscience*, 5 (2015) 569-581.

[41] O. Anwar Bég, Tasveer A. Bég, N. Raheem and W. Iqbal, **BAC-FLOW** - Finite element simulation program for slimy dynamics of micro-organisms in surface coating anti-biofouling applications with benchmarking for CFD, *Technical Report, GORT-MAR-BIO-A763, 161pp, Prepared for Norwegian offshore industry consortium, Trondheim, June* (2013).

[42] S.S. Rao, *The Finite Element Method in Engineering*, Elsevier, USA, 4th Edn. (2004).

FIGURES

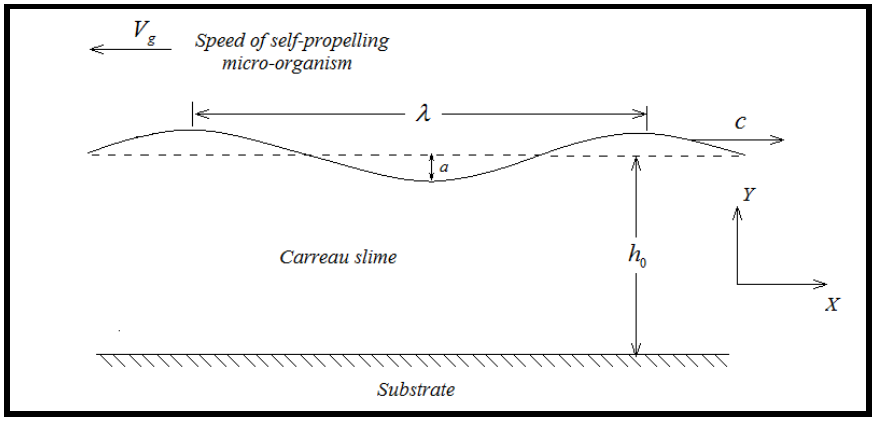

Fig.1. Diagram of undulating surface model.

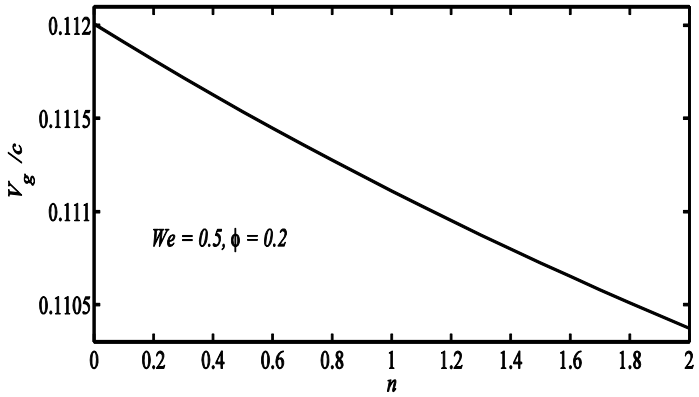

(a)

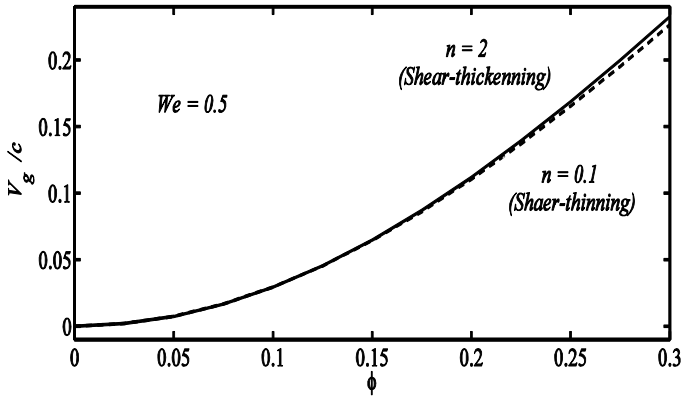

(b)

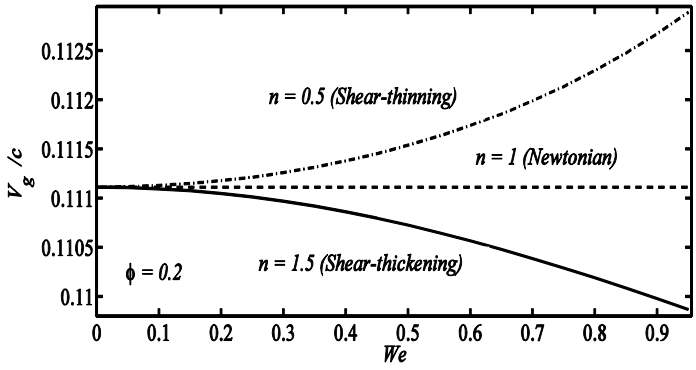

(c)

Fig. 2. Plots of the variation the speed of the gliding organism in the moving frame with respect to different involved parameters.

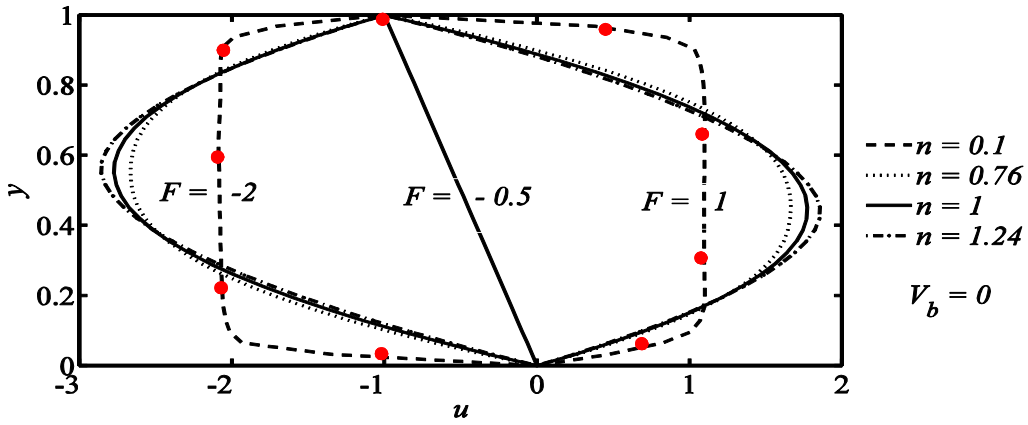

Fig. 3. (a) Plots of velocity profile for various values of n and F at a position of $h=1$. The relative speed of the substrate is fixed as $V_b=0$ and the Weissenberg number $We=7$.

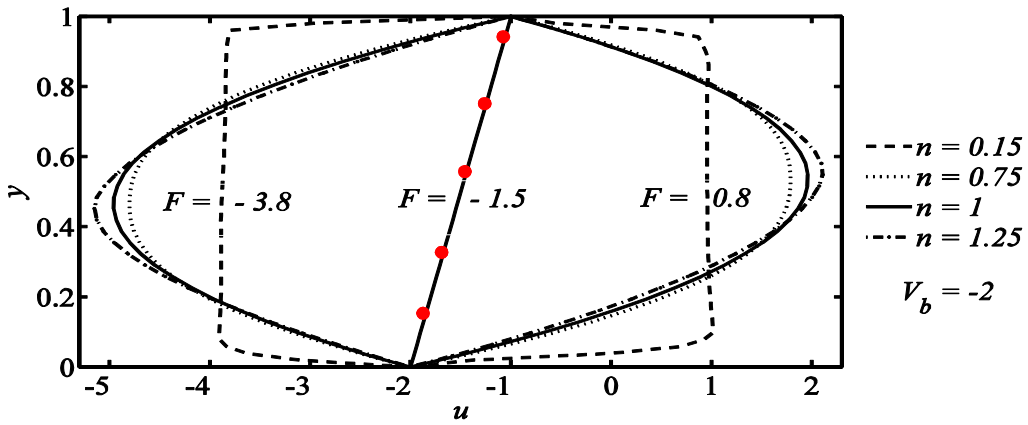

Fig. 3. (b) Plots of velocity profile for various values of n and F at a position of $h=1$. The relative speed of the substrate is fixed as $V_b=-2$ and the Weissenberg number $We=6$.

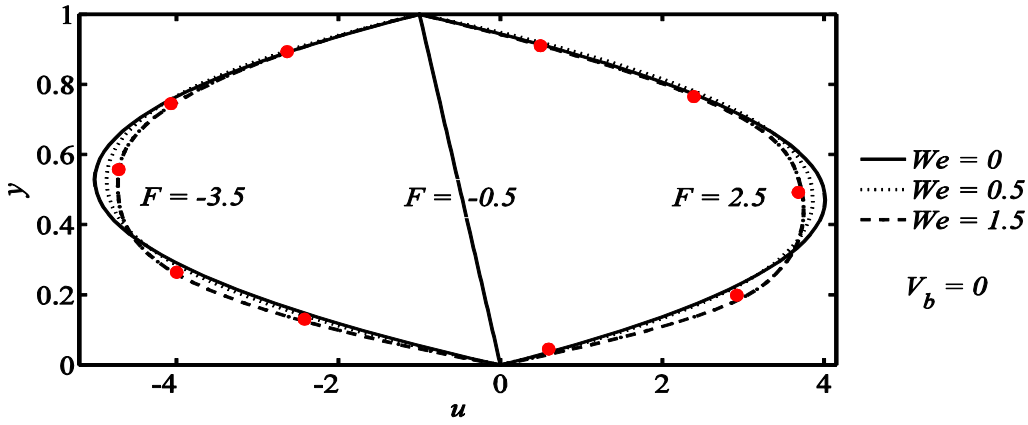

Fig. 4. (a) Plots of velocity profile for various values of We and F at a position of h =1. The relative speed of the substrate is fixed as $V_b=0$ and for thinning effects $n=0.8$.

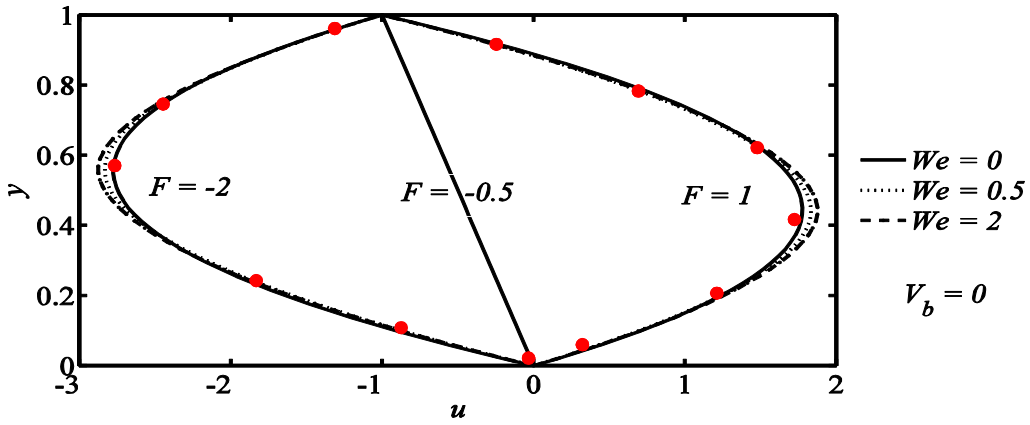

Fig. 4. (b) Plots of velocity profile for various values of We and F at a position of h =1. The relative speed of the substrate is fixed as $V_b = 0$ and for thickening effects $n = 1.2$.

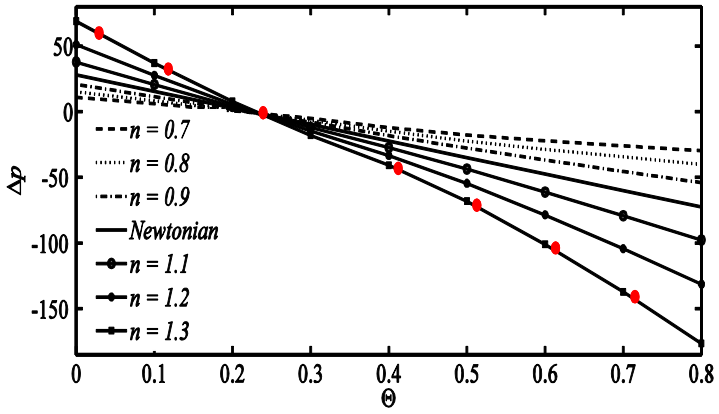

Fig. 5. Plots of pressure rise per wavelength Δp versus flow rate Θ for various values of n. The other parameters are: $We = 5$, $V_b = -1$.

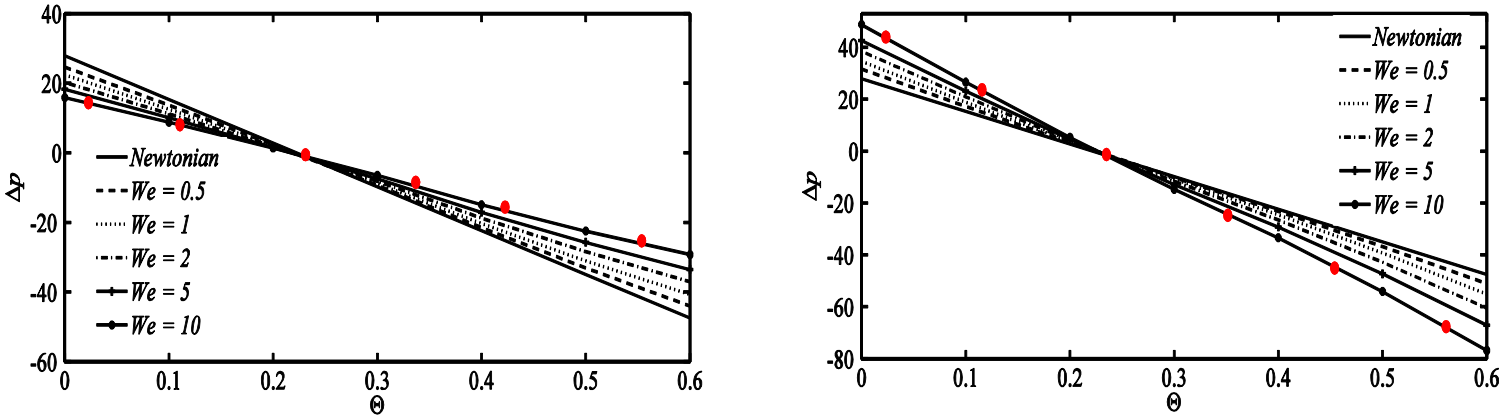

Fig. 6. Plots of pressure rise per wavelength Δp versus flow rate Θ for various values of We. Panel (a) $n = 0.85$ (thinning) and panel (b) $n = 1.15$ (thickening). Here $V_b = -1$.

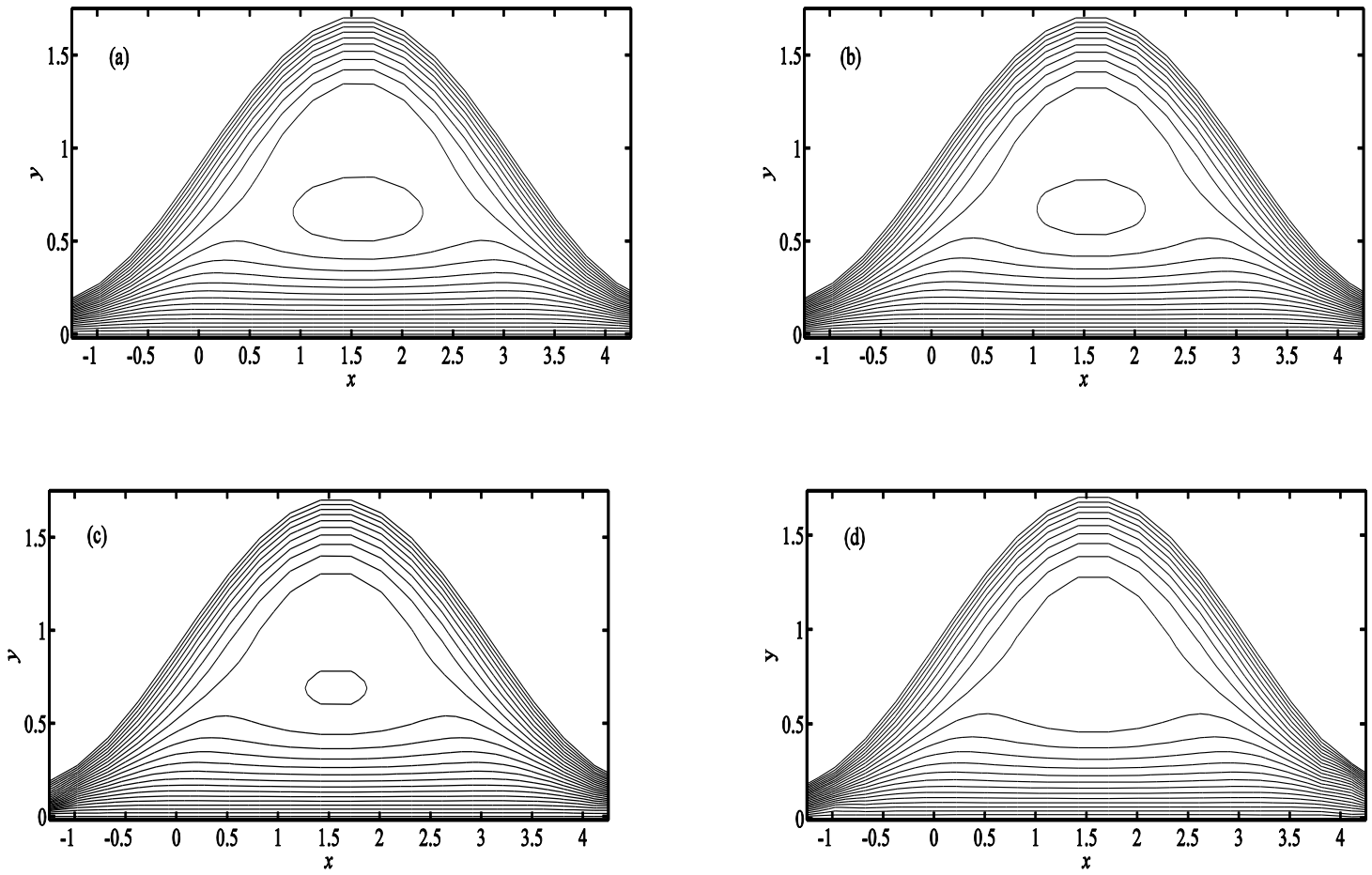

Fig. 7. Streamlines for different values of We. Panels (a)-(d) corresponds to the values. $We = 0\left(Newtonian\right)$, $We = \left(0.5,\ 1,\ 2\right)$ respectively. The other parameters are: $F = -0.5,\ V_b = -1,\ n = 0.7$.

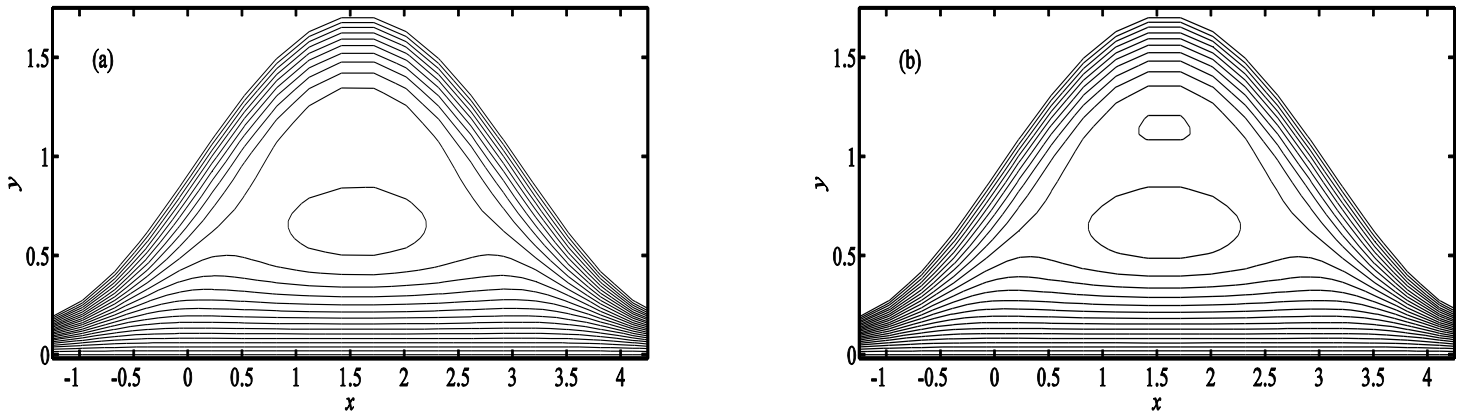

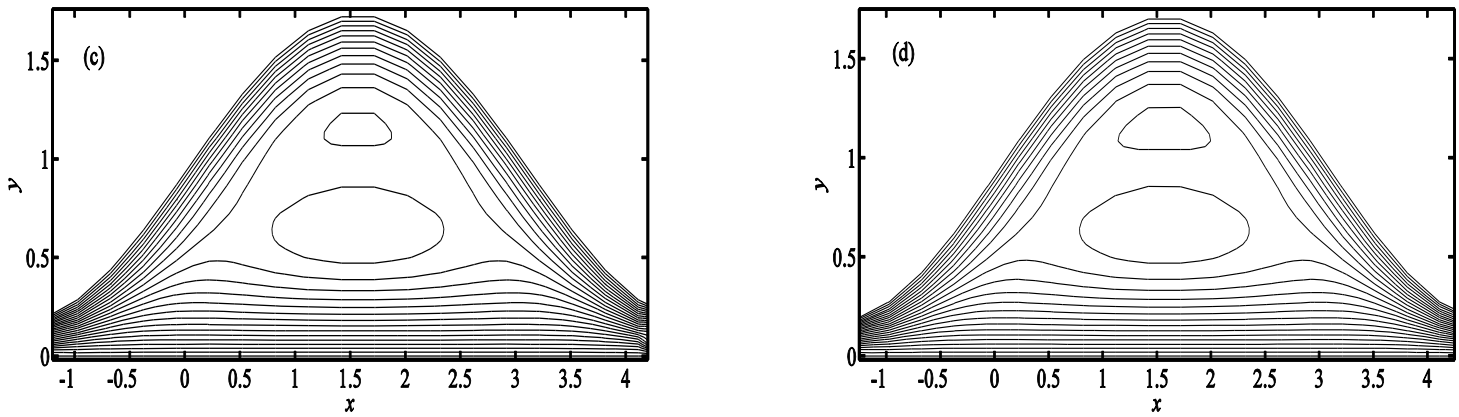

Fig. 8. Streamlines for different values of We. Panels (a)-(d) corresponds to the values. $We = 0\left(Newtonian\right)$, $We = \left(0.5,\ 1,\ 2\right)$ respectively. The other parameters are: $F = -0.5,\ V_b = -1,\ n = 1.2.$

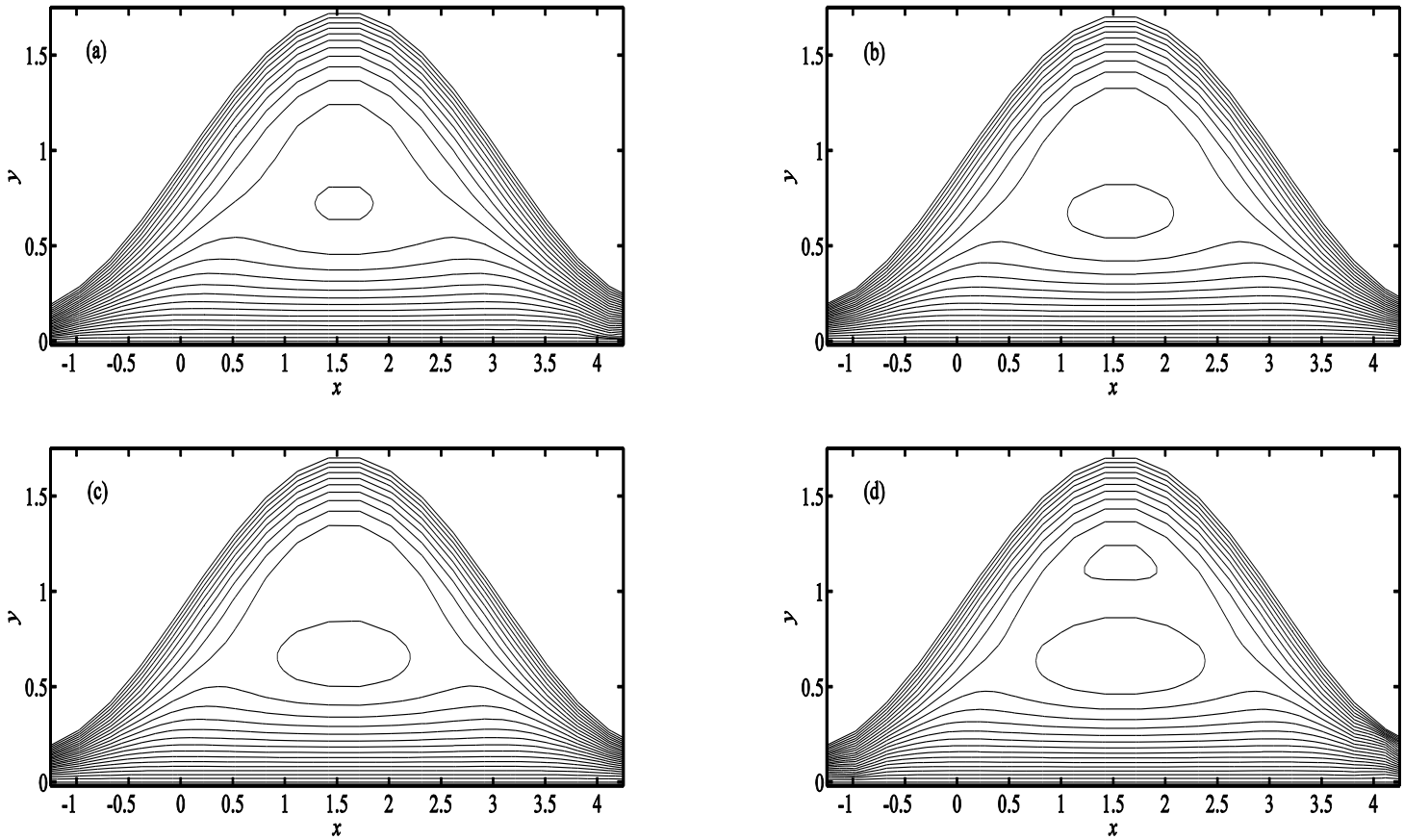

Fig. 9. Streamlines for different values of n. Panels (a)-(d) corresponds to the values. $n = \left(0.2,\ 0.7,\ 1,\ 1.5\right)$ respectively. The other parameters are: $F = 0.5,\ V_b = -1,\ We = 0.5.$

APPENDIX

A. PERTURBATION EXPANSION SOLUTION

For small values of $We,$ Eqns. (25) and (26) give:

$$\frac{\partial^2}{\partial y^2}\left[\left(1+We^2\left(\frac{n-1}{2}\right)\left(\frac{\partial^2\psi}{\partial y^2}\right)^2\right)\left(\frac{\partial^2\psi}{\partial y^2}\right)\right]=0, \tag{A1}$$

$$\frac{\partial p}{\partial x}=\frac{\partial}{\partial y}\left[\left(1+We^2\left(\frac{n-1}{2}\right)\left(\frac{\partial^2\psi}{\partial y^2}\right)^2\right)\left(\frac{\partial^2\psi}{\partial y^2}\right)\right]. \tag{A2}$$

In the interest of deriving an approximate solution valid for small Weissenberg number, we write ψ, p and F in the following power series expansion form:

$$\begin{aligned}\psi &= \psi_0 + We^2\psi_1 + \dots,\\ p &= p_0 + We^2 p_1 + \dots,\\ F &= F_0 + We^2 F_1 + \dots.\end{aligned} \tag{A3}$$

Now, performing the usual perturbation analysis [15], it is possible to extract the following expressions for stream function, longitudinal velocity, pressure gradient and pressure rise per wavelength, respectively:

$$\begin{aligned}\psi = {} & \frac{y\left[\left(3h-2y\right)yF_0+h\left(h-y\right)\left(y+\left(h-y\right)V_b\right)\right]}{h^3}+We^2\frac{\left(n-1\right)y^2}{5h^9}\left[-108\left(h-2y\right)\left(h-y\right)^2F_0^3\right.\\ & \left.-9\left(V_b-1\right)K_1\left(x,y\right)+36K_2\left(x,y\right)+h^3\left(5\left(3h-2y\right)F_1h^3/\left(n-1\right)+9\left(V_b-1\right)^2K_3\left(x,y\right)\right)\right],\end{aligned} \tag{A4}$$

$$\begin{aligned}u = {} & \frac{h\left(2h-3y\right)y+\left(h-y\right)\left(6yF_0+h\left(h-3y\right)V_b\right)}{h^3}+We^2\frac{3\left(n-1\right)\left(h-y\right)y}{5h^9}\left[-72\left(h^2-5hy+5y^2\right)F_0^3\right.\\ & \left.+12K_4\left(x,y\right)-6\left(V_b-1\right)K_5\left(x,y\right)+h^3\left(10h^3F_1/\left(n-1\right)+3\left(V_b-1\right)^2K_6\left(x,y\right)\right)\right],\end{aligned} \tag{A5}$$

$$\frac{dp}{dx}=-\frac{6\left(h+2F_0-hV_b\right)}{h^3}-We^2\frac{36}{h^9}\left(n-1\right)\left(h+2F_0-hV_b\right)\left[3\left(h-2y\right)F_0+h\left(h-3y+\left(3y-2h\right)V_b\right)\right]^2, \tag{A6}$$

$$\Delta P_{\lambda} = -12\mathrm{I}_3 F_0 - 6\mathrm{I}_2\left(1-V_b\right) + We^2\frac{(n-1)}{5}\Big[-648I_7F_0^3 - 12I_3F_1 + 972I_6F_0^2\left(V_b-1\right) \\ -72\mathrm{I}_5F_0\left(8+V_b\left(8V_b-11\right)\right) + 18\mathrm{I}_4\left(V_b-1\right)\left(7+V_b\left(7V_b-4\right)\right)\Big]. \tag{A7}$$

Here:

$$I_2 = \frac{2\pi}{\left(1-\phi^2\right)^{3/2}}, \quad I_3 = \frac{\pi\left(2+\phi^2\right)}{\left(1-\phi^2\right)^{5/2}}. \tag{A8}$$

$$I_n = \frac{1}{\left(1-\phi^2\right)}\left[\left(\frac{2n-1}{n-1}\right)I_{n-1} - \left(\frac{n-2}{n-1}\right)I_{n-2}\right],\ n>4. \tag{A9}$$

$$\begin{aligned}
K_1(x,y) &= h^2\left(h-y\right)^2F_0\left(h+18y+\left(19h-18y\right)V_b\right)\\
K_2(x,y) &= h\left(h-y\right)^2F_0^2\left(-2h+9y+\left(7h-9y\right)V_b\right)\\
K_3(x,y) &= \left(h-y\right)^2\left(h+3y+\left(4h-3y\right)V_b\right)\\
K_4(x,y) &= hF_0^2\left(-4h^2+35hy-45y^2+\left(14h^2-55hy+45y^2\right)V_b\right)\\
K_5(x,y) &= h^2F_0\left(h^2+25hy-45y^2+\left(19h^2-65hy+45y^2\right)V_b\right)\\
K_6(x,y) &= \left(2h^2+5hy-15y^2+\left(8h^2-25hy+15y^2\right)V_b\right)
\end{aligned} \tag{A10}$$

Now using the relation $F_0 = F^{(1)} - We^2F_1$ in (A7) and retaining the terms of order We^2, one gets the expression (29).

The dimensionless formulae defining the *horizontal* and *vertical* forces *per unit width per wavelength* on the surface of the organism are given by:

$$F_x = \int_0^{2\pi}\tau_x\big|_{y=h}\,dx, \quad F_y = \int_0^{2\pi}\tau_y\big|_{y=h}\,dx, \tag{A11}$$

Here τ_x and τ_y are the component of stress vectors $\boldsymbol{\tau}$ given by:

$$\tau_x = -p\frac{\partial h}{\partial x} + S_{xy} \quad \text{and} \quad \tau_y = -p + S_{yy}. \tag{A12}$$

We refer the reader to ref. [14] for detailed derivation of above the formulae which is omitted here for brevity. On substituting the values of τ_x and τ_y in (A11) and using the relation $F_0 = F^{(1)} - We^2F_1,$ one readily obtain the expressions (30) and (31).

The non-dimensional expression for power required for gliding of the organism at a steady speed V_b is calculated by:

$$P = \int_0^{2p} \left(\tau_x u + \tau_y v \right) \Big|_{y=h} dx. \tag{A13}$$

In term of dimensionless stream function the above expression becomes:

$$P = \int_0^{2p} \left(\frac{\partial y}{\partial y} \tau_x + \frac{\partial y}{\partial x} \tau_y \right) \Big|_{y=h} dx, \tag{A14}$$

In view of the long wavelength assumption, the expression (A14) readily contracts to:

$$P = \int_0^{2p} \frac{\partial y}{\partial y} t_x \Big|_{y=h} dx. \tag{A15}$$

According to Eqns. (27) and (A11), Eqn. (A15) gives the expression (32).

B. FINITE DIFFERENCE METHOD (FDM) NUMERICAL COMPUTATIONS

A numerical solution of the boundary value problem consisting of Eq. (25) and boundary conditions (27) provides validation of the perturbation solutions for large values of the hydrodynamic parameters. To this end, we shall employ an implicit iterative finite difference method (FDM). We construct an iterative procedure to convert the original nonlinear problem to a linear one at the $(m+1)^{\text{th}}$ iterative step, as follows:

$$g^{(\mathrm{m})} \frac{\partial^4 \psi^{(m+1)}}{\partial y^4} + \frac{\partial g^{(\mathrm{m})}}{\partial y} \frac{\partial^3 \psi^{(m+1)}}{\partial y^3} + \frac{\partial^2 g^{(\mathrm{m})}}{\partial y^2} \frac{\partial^2 \psi^{(m+1)}}{\partial y^2} = 0, \tag{A16}$$

$$\begin{aligned} &\psi^{(m+1)} = 0, \quad \frac{\partial \psi^{(m+1)}}{\partial y} = V_b \quad at \;\; y = 0, \\ &\psi^{(m+1)} = F, \quad \frac{\partial \psi^{(m+1)}}{\partial y} = -1 \quad at \;\; y = h, \end{aligned} \tag{A17}$$

where

$$g^{(\mathrm{m})}(y)=\left(1+We^{2}\left(\frac{\partial^{2}\psi^{(\mathrm{m})}}{\partial y^{2}}\right)^{2}\right)^{\frac{n-1}{2}}. \tag{A18}$$

Here the superscript (m) denotes the iterative step. It is now clear that the above boundary value problem is linear in $\psi^{(m+1)}$. Inserting finite-difference approximations of $\psi^{(m+1)}$ and its derivative in Eq. (25) and boundary conditions given in Eq. (27), a system of linear algebraic equations may be obtained and solved for each iterative $(m+1)^{\text{th}}$ step. In this way numerical values of $\psi^{(m+1)}$ at each cross-section can be obtained. Of course some suitable initial numerical values of $\psi^{(m)}$ are specified at each cross-section to start the iterative procedure. Unfortunately by increasing the number of iterations a convergent solution is *not always possible*, especially when initial numerical values of ψ are not prescribed carefully. In such circumstances the method of *successive under-relaxation* is used. In this method the estimated value of ψ at (m+1) iterative step i.e. $\tilde{\psi}^{(m+1)}$ is refined to achieve the convergent value of ψ at the same step. This can achieved by the following formula:

$$\psi^{(m+1)}=\psi^{(m)}+\tau\left(\tilde{\psi}^{(m+1)}-\psi^{(m)}\right). \tag{A19}$$

where $\tau\in(0,1]$ is an *over-relaxation* parameter. It is also pertinent to select τ as sufficiently small such that convergent iteration is readily attained. The iteration in this problem is carried out to calculate the value of ψ convergent to 10^{-8}. The above method has earlier been successfully implemented by Wang *et al.* [16] and also Hayat *et al.* [17] in the context of gliding motility of bacteria showing excellent accuracy and stability.

C. VALIDATION WITH VARIATIONAL FINITE ELEMENT METHOD (FEM)

The nonlinear two-point boundary defined by eqn. (25) and boundary conditions (27) has also been solved with a third approach, namely the finite element method. To this end the same F and V_b values are prescribed in the boundary conditions as employed in the FDM computations. The formulation adopted is "weak" and particularly suited to fluid dynamics phenomena. It has been applied quite recently also to simulate many diverse problems in for example nanofluid solar

energy collector heat transfer [36], biomagnetic transport phenomena in tissue [37], polymeric fluid dynamics [38], hemodynamics [39] and magnetic smart materials [40]. The code, **BAC-FLOW** [41] has been customized to simulate gliding bacterial rheological flows. Following some numerical tests, mesh-independence is confirmed for the present scenario with 100 finite elements. The whole domain is therefore discretized into a set of 100 line elements of equal width, each element being *two-noded*. Line elements are sufficient since only one spatial variable i.e. normalized radial coordinate, y is involved. A variational form is derived for the eqn. (25) in which the non-dimensional stream function, ψ, is the *master dependent variable*. Numerical integration is performed over the artificial finite element domain in terms of the normalized coordinate (y_e; y_e+1) using arbitrary test functions (W_1, W_2) which can be viewed as the variation in the master variables. The nonlinear terms in eqn. (25) are easily accommodated. The finite element form of the variational equations is achieved by appropriate substitutions based on the following approximation:

$$\Psi = \sum_{j=1}^{2} w_j \psi_j \tag{A20}$$

Here Ψ represents ψ (stream function). With the following definitions for weighting functions [42]:

$$W_1 = W_2 = \Psi_i, \quad i = 1,2 \tag{A21}$$

The shape (interpolation) functions for a typical line element (y_e, y_{e+1}) in eqn. (56) are prescribed as follows:

$$\Psi_1^{(e)} = \frac{y_{e+1} - y}{y_{e+1} - y_e}; \ \Psi_2^{(e)} = \frac{y - y_e}{y_{e+1} - y_e}, \ y_e \le y \le y_{e+1} \tag{A22}$$

The *matrix-vector* form of the finite element model is then generated. Comprehensive details are given in [36-42]. This system of non-linear algebraic equations produced after assembly of the element equations is linearized by incorporating the stream function ψ which is assumed to be known. The collection of elements is called *the finite-element mesh* or grid. The element matrix, which is called a *stiffness matrix*, is constructed by using *element interpolation functions*. The algebraic equations so obtained are assembled by imposing the inter-element continuity

conditions. This yields a large number of algebraic equations defining the *global finite element model*, which governs the whole domain. The essential and natural boundary conditions are imposed on the assembled equations. The assembled equations so obtained can be solved by any "matrix" numerical technique e.g. Householder's approach, LU Decomposition method, Choleski decomposition etc. Criteria for the selection for elements are also documented in Rao [42]. The non-linear algebraic system of equations is solved iteratively. An accuracy of 0.00000001 is used. A convergence criterion based on the relative difference between the current and previous iterations is employed. When these differences reach the desired accuracy, the solution is assumed to have converged and the iterative process is terminated. Two-point Gaussian quadrature is implemented for solving the integrations. The **BAC-FLOW** FEM algorithm has been executed in **MATLAB** running on an Octane SGI desktop workstation and takes 10-15 seconds to converge. We note that in **Figs. 3-6** the red filled circles denote the **FEM** solutions. In each figure one particular case for either *F, n* or *We* has been validated. Excellent correlation is obtained for all cases included (indicated by red filled circles in the respective plots). Confidence in the **FDM** code is therefore justifiably high.